

Degradation Mechanisms Investigation for Long-term Thermal Stability of Dye-Sensitized Solar Cells

Guogang Xue^{1,2}, Yong Guo¹, Tao Yu^{1,*}, Jie Guan¹, Xirui Yu¹, Jiyuan Zhang¹, Jianguo Liu^{1,3}, Zhigang Zou^{1,3}

¹ Eco-materials and Renewable Energy Research Center, School of Physics, National Laboratory of Solid State Microstructures, Nanjing University, Nanjing 210093, China

² School of Physics and Electronic Engineering, Jiangsu Normal University, Xuzhou 221116, China

³ Department of Materials Science and Engineering, Nanjing University, Nanjing 210093, China

*E-mail: yutao@nju.edu.cn

Received: 3 January 2012 / Accepted: 21 January 2012 / Published: 1 February 2012

This paper describes a systematic study on exploring and understanding degradation mechanisms for long-term thermal stability of dye-sensitized solar cells (DSSCs). A 1080-hour thermal stability testing of DSSCs was conducted. Two different temperature conditions were selected to deeply explore the degradation mechanisms of DSSCs performance. One temperature condition is at 25°C, the other is under a temperature cycle from -20°C to 25°C. DSSCs were sensitized by bis(tetrabutylammonium) *cis*-bis(thiocyanato)bis(2,2'-bipyridine-4-carboxylic acid, 4'-carboxylate)ruthenium(II) (N719). The cells maintained ca. 80% of its initial overall power conversion efficiency (η) after 1080-hour aging. It is found that the decrease of η was ascribed to the decrease of short-circuit current density (J_{SC}) while the open-circuit photovoltage and the fill factor increased with time; and the decrease rate of J_{SC} for the cell under the temperature cycle from -20°C to 25°C was slower, compared with the cell at 25°C. From the physical point of view, the reason for the drop in J_{SC} was analyzed. Several possible degradation mechanisms, which are stability of the dye, aging of the photoelectrode film, change of the electrolyte components, and degradation of the counter electrode, were discussed systematically. Particularly, the long-term stability of N719 adsorbed on the TiO₂ electrode permeated in the electrolyte was investigated by using UV-visible absorption spectrum and resonance Raman scattering. Density functional theory calculations were applied to illustrate the deterioration of N719 which caused the decrease of the light harvesting efficiency of photoelectrode and subsequently decreased J_{SC} . Moreover, high temperature will accelerate the deterioration. Additionally, the change of the electron transport/transfer between the interfaces in DSSCs, which was caused by aging of the photoelectrode film, change of the electrolyte components, and degradation of the counter electrode, was analyzed with electrochemical impedance spectroscopy (EIS). The analysis result of EIS shows that the change of the electron collection efficiency of photoelectrode with time was not large. As a conclusion, the long-term stability of N719 is found to be the main reason for DSSCs degradation.

Keywords: dye-sensitized solar cells, thermal stability, N719, photoelectrode film, EIS

1. INTRODUCTION

Dye-sensitized solar cells (DSSCs) have drawn much attention since 1991 [1-3]. DSSCs present a promising alternative to conventional pn-junction solar cells due to the low cost and flexible fabrication. Recently, a conversion efficiency of 12.3% on small area was reported under AM 1.5 global illumination [4]. However, the challenge of long-term stability has to be faced and overcome before DSSCs successfully enter into the photovoltaic market for application. Among a large quantity of publications on DSSCs during the past decade, few papers have focused on long-term stability of DSSCs [5,6]. These papers mostly pay attention to the influences of illumination conditions, temperature, humidity, and outdoor condition [7-15]. M. Grätzel has reported small cells endure 1000 h of aging at 80°C in the dark and AM 1.5 illumination of visible light at 60°C with minor performance degradation [7]. Dai et al. have designed the large area modules and a 500 W primary DSSCs power station then studied their stability and performance under outdoor condition [10]. A combination of 85°C in the dark and full sun illumination leads to a significant decrease of the large cell performance, which has been reported by P. M. Sommeling and his coworkers [14]. It is shown that temperature is an important factor to be studied for long-term stability investigation of DSSCs.

Some papers have started to explore the mechanisms influenced the stability of DSSCs. Hagfeldt's group has studied the mechanisms of the thiocyanato ligand exchange reactions between the redox couple Γ/I_3^- and the ruthenium complex bis(tetrabutylammonium) *cis*-bis(thiocyanato)bis(2,2'-bipyridine-4-carboxylic acid, 4'-carboxylate)ruthenium(II) (N719) [16]. M. Toivola et al. analyzed the effects of aging and cyclically varying temperature on the electrical parameters of DSSCs with electrochemical impedance spectroscopy (EIS) [8]. Using Raman spectroscopy in addition to EIS, N. Kato et al. have clarified the deteriorated components of DSSCs module after the long durability test and analyzed the change of the components in the electrolyte [15]. Based on these works, a systematic study on degradation mechanisms for long-term thermal stability of DSSCs is necessary to be conducted. Certainly, there is a need for a deep analysis to better understand how the degradation mechanisms influence the photoelectric parameters of DSSCs.

This work investigated a 1080-hour thermal stability testing of DSSCs sensitized by N719. Two different temperature conditions were selected to deeply explore the degradation mechanisms of DSSCs performance. One temperature condition is at 25°C (i.e. room temperature), the other is under a temperature cycle from -20°C to 25°C. The room temperature is similar to laboratory condition and the temperature cycle is closer to outdoor condition for practical application, especially in the high-latitude zone. From stability of the dye, aging of the photoelectrode film, change of the electrolyte components, and degradation of the counter electrode, a systematic study on degradation mechanisms for DSSCs aged 1080 h was conducted. Particularly, the long-term stability of N719 adsorbed on the nanoporous TiO₂ electrode film permeated in the electrolyte was investigated by using UV-visible absorption spectrum and resonance Raman scattering. Density functional theory calculations were applied to illustrate the deterioration of N719 which caused the decrease of the light harvesting efficiency of photoelectrode and subsequently decreased the short-circuit current density. Additionally, the change of the electron transport/transfer between the interfaces in DSSCs, which was ascribed to aging of the photoelectrode film, change of the electrolyte components, and degradation of the counter electrode,

was analyzed with EIS. The analysis result of EIS shows that the change of the electron collection efficiency of photoelectrode with time was not large. The details are discussed in later sections.

2. EXPERIMENTAL SECTION

2.1. Fabrication of DSSCs

A previously cleaned fluorine-doped tin oxide (FTO) conductive glass ($15 \Omega/\square$) was treated by a 40 mM TiCl_4 aqueous solution at 70°C for 30 min using chemical bath deposition method to deposit a thin TiO_2 particle compact layer. The pre-prepared P25 TiO_2 paste [17] was coated on this FTO conductive glass substrate using the doctor blade technique. The TiO_2 electrode was gradually sintered in a furnace under an air flow. The heating program was provided as: 125°C for 60 min, 325°C for 5 min, 375°C for 5 min, 450°C for 15 min, and 500°C for 15 min. After cooling down, the TiO_2 electrode was further treated by a 40 mM TiCl_4 aqueous solution at 70°C for 30 min and calcined at 500°C for 30 min. When the temperature was cooled down to 80°C , the TiO_2 electrode was immersed into a ruthenium dye solution (0.5 mM N719, Solaronix, in ethanol) for 24 h in the dark, and the excess amount of dye was then rinsed off with ethanol. Thus, a transparent film of interconnected TiO_2 particles adsorbing the N719 dye was fabricated as a photoelectrode (PE). Another FTO glass substrate deposited a thin Pt layer by the ion sputtering method was used as a counter electrode (CE). The two electrodes were sealed with a 25 μm thick Surlyn film (DuPont) at 110°C for 30 s, and an electrolyte solution was filled through arbitrary one of two pre-drilled holes on the counter electrode. Each of the holes was then sealed immediately by sandwiching a Surlyn film between the CE substrate and a microscope slide. The electrolyte consists of 0.6 M 1-butyl-3-methylimidazolium iodide (BMII), 0.03 M iodine, 0.06 M lithium iodide, 0.5 M 4-*tert*-butylpyridine, and 0.1 M guanidinium thiocyanate in a solution of acetonitrile/valeronitrile (85:15, v/v). Figure 1 shows a complete dye-sensitized solar cell made by our research group.

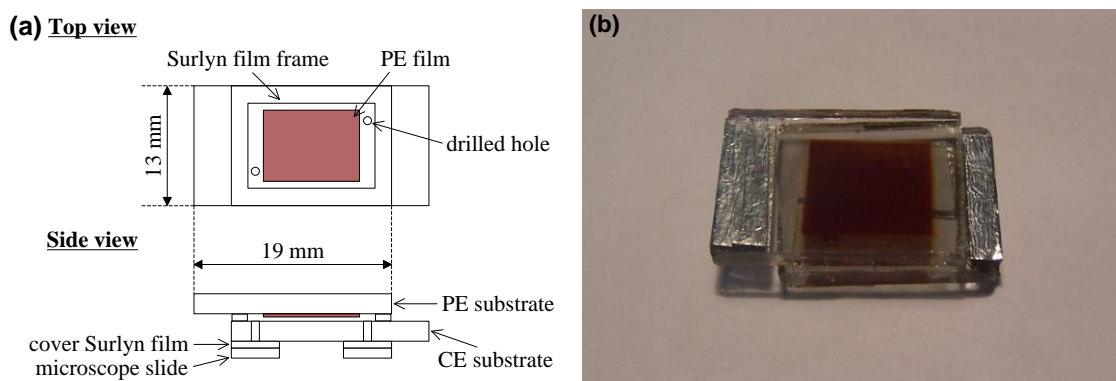


Figure 1. Schematic diagram (a) of a small area laboratory DSSC and a picture (b) of the laboratory DSSC sample.

2.2. Density functional theory (DFT) calculations

All calculations were performed with B3LYP method [18,19] in Gaussian 03 program [20]. LanL2DZ basis set was used to for Ru atom, and 3-21G* basis set was applied to all of the rest atoms [21]. The highest occupied molecular orbital (HOMO) and the lowest unoccupied molecular orbital (LUMO) were constructed with Gview program based the optimized results.

2.3. Measurements

The current-voltage (I - V) measurements were carried out with an active area of 0.132 cm² by a Keithley 236 source measure unit under AM 1.5 global simulated sunlight (100 mW/cm²) which was produced by a 150 W Oriel Solar Simulator (92251A, ASTM class A). The incident light intensity was calibrated to 1 sun by a photovoltaic reference cell system (91150, Oriel instruments, USA). The conversion efficiency η of the solar cell is calculated from the short-circuit photocurrent density (J_{SC}), the open-circuit photovoltage (V_{OC}), the fill factor (FF), and the intensity of the incident light (I_{ph}),

$$\eta = (J_{SC} \cdot V_{OC} \cdot FF) / I_{ph} \quad (1)$$

The incident photon to electron conversion efficiency (IPCE) of a DSSC was measured at the short-circuit condition with a computerized apparatus (Chinese patent ZL200910233754.0) consisting of a 1000 W xenon lamp (66359, Oriel instruments, USA) coupled to a 1/2 m monochromator (Omni- λ 500, Zolix, China), a Keithley 2400 digital source meter, and a Newport 1918-C power meter with a Newport 818-ST-UV detector head. A 6-position filter wheel (SD, Zolix, China) was inserted in the incident light beam to remove the second order diffraction. The wavelength scanning range was from 300 nm to 800 nm with the interval of 10 nm. At each measuring wavelength, three seconds was needed to wait the incident monochromatic light getting stable. The cell was illuminated from the PE side. The IPCE value is calculate from the formula,

$$IPCE(\lambda) = \frac{1240 J_{SC}(\lambda)}{\lambda P_{in}(\lambda)} \quad (2)$$

where λ is the incident monochromatic light wavelength (nm), J_{SC} is the short-circuit photocurrent density (mA/cm²), and P_{in} is the incident monochromatic light intensity (mW/cm²).

The EIS measurements were carried out with a PARSTAT 2273 advanced electrochemical system (Princeton Applied Research, USA) over a frequency range of 10⁻¹-10⁵ Hz at room temperature. The magnitude of ac modulation signal was 10 mV. All the measurements applied bias of V_{OC} under AM 1.5 global illumination. ZView software (v3.1, Scribner Associate, Inc.) was used to analyzing the impedance spectroscopy.

The micro-Raman spectrometer (JY-HR800, France) equipped with a 488 nm Ar⁺ laser was used in recording the resonance Raman scattering (RRS) spectra of DSSCs. The spectral range was of 100-3000 cm⁻¹ with 0.5 cm⁻¹ resolution.

The N719 dye was desorbed from the TiO₂ electrode film by immersing it in a 0.05 M NaOH aqueous solution. Then the UV-visible absorption spectrum (UV-vis) of the dye solution was recorded on a Varian Cary 50 UV-visible spectrophotometer.

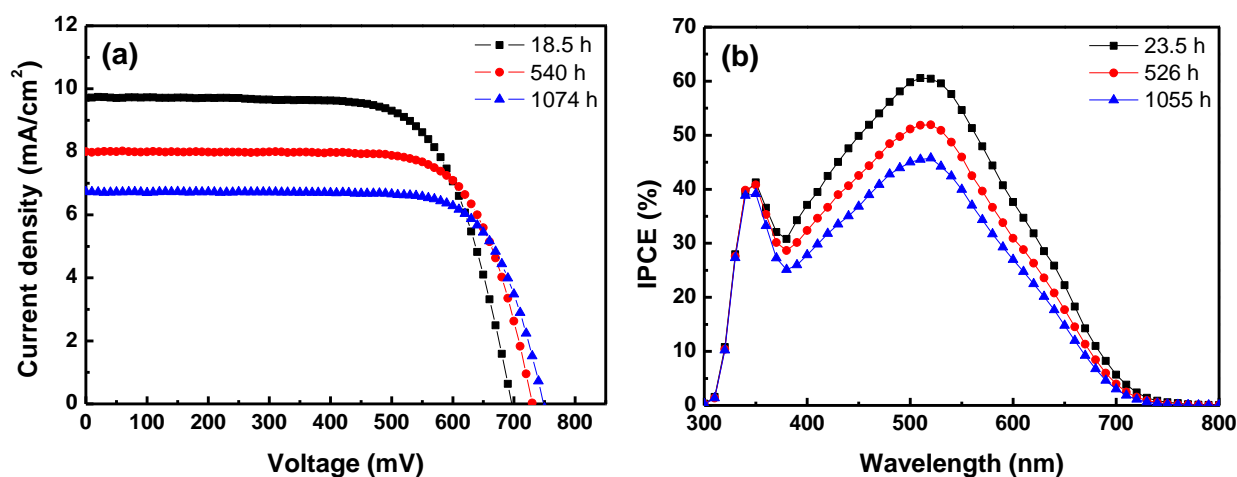
A field-emission scanning electron microscope (Nova NanoSEM 230, FEI, USA) was applied to observing the TiO₂ photoelectrode films. The thickness of TiO₂ photoelectrode film was measured by a Dektak 6M profilometer.

2.4. Endurance test of DSSCs

Three DSSCs were fabricated. The DSSC stored at 25°C was denoted as Cell A, and the DSSC, denoted as Cell B, was stored under the environment subjected to a temperature cycle of -20°C for 12 h and subsequently 25°C for 24 h. Cell A was stored in the electronic moistureproof box with a constant humidity of 25%. Cell B was firstly stored in a freezer for 12 h and then in the electronic moistureproof box for 24 h. Cell B was sealed in two nested polyethylene ziplock bags before it was put in the freezer. A long-term stability experiment of 1080 h was conducted for the two cells. This means that Cell B experienced 30 temperature cycles. Both cells were subjected to such measurements as: *I-V*, IPCE, EIS, UV-vis and scanning electron microscopy (SEM) at 25°C. For comparison, a new TiO₂ electrode was prepared and characterized with UV-vis and SEM. Another DSSC, denoted as Cell C, was characterized with RRS after stored in the electronic moistureproof box at 25°C for 4 months.

3. RESULTS AND DISCUSSION

3.1. Long-term photovoltaic performance



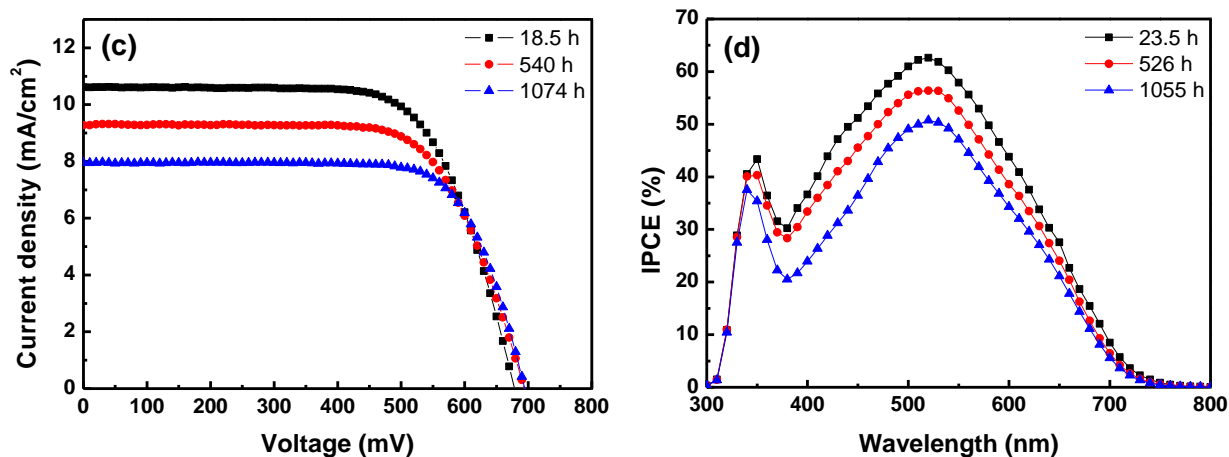


Figure 2. *I-V* characteristics (a) and IPCE spectra (b) of Cell A aged at 25°C; *I-V* characteristics (c) and IPCE spectra (d) of Cell B aged under the temperature cycle from -20°C to 25°C.

I-V curves and IPCE spectra of Cell A and Cell B vs. the testing time are shown in Figure 2. It gives the curves of three testing points. Table 1 gives the specific parameters of *I-V* curves including J_{SC} , V_{OC} , FF and η as well as the thickness (d) of TiO_2 photoelectrode film.

The PE film of Cell B was thicker than that of Cell A, which promoted the light absorption of Cell B. This just explains the reason why the initial J_{SC} of Cell B was higher than that of Cell A [22]. For Cell A, J_{SC} at 1074 h decreased to 69.4% of J_{SC} at 18.5 h, V_{OC} at 1074 h increased to 107.5% of V_{OC} at 18.5 h, FF at 1074 h increased to 106.0% of FF at 18.5 h, η at 1074 h decreased to 79.0% of η at 18.5 h; and for Cell B, J_{SC} at 1074 h decreased to 75.1% of J_{SC} at 18.5 h, V_{OC} at 1074 h increased to 102.4% of V_{OC} at 18.5 h, FF at 1074 h increased to 106.4% of FF at 18.5 h, η at 1074 h decreased to 81.9% of η at 18.5 h.

These data indicate that: (1) the considerable decrease of J_{SC} resulted in the decrease of η for both cells. On the other hand, the increase of V_{OC} and FF slowed the decrease of η ; (2) J_{SC} of Cell A decreased more than that of Cell B, while V_{OC} of Cell A increased more than that of Cell B, and the increase of FF was almost the same for the two cells.

Additionally, it can be seen that accompanying with the considerable drop of J_{SC} for the two cells, the corresponding IPCE spectra values also dropt considerably with time. It is pretty widely known that J_{SC} under AM 1.5 global illumination can be calculated by integrating the product of the incident monochromatic photon flux density ($F(\lambda)$) of AM 1.5 global solar spectrum and $IPCE(\lambda)$ of the cell over the wavelength (λ) of the incident light,

$$J_{SC} = q \int IPCE(\lambda) F(\lambda) d\lambda \quad (3)$$

where q is the elementary charge. Thus, the downward trends with time in J_{SC} and IPCE spectra were consistent.

Table 1. *I-V* specific parameters of Cell A and Cell B.

Device	<i>d</i> (μm)	Duration of time (h)	<i>J</i> _{SC} (mA/cm ²)	<i>V</i> _{OC} (mV)	<i>FF</i> (%)	<i>η</i> (%)
Cell A	7.6	18.5	9.70	697	70.4	4.76
		540	8.02	730	73.1	4.28
		1074	6.73	749	74.6	3.76
Cell B	10	18.5	10.59	679	69.1	4.96
		540	9.28	694	69.4	4.47
		1074	7.95	695	73.5	4.06

Figure 3 shows the evolution curve of each *I-V* parameter about the two DSSCs. For both cells, *J*_{SC} had a linear downward process. Fitting the *J*_{SC} data, the slope is -2.53×10^{-3} for Cell A and -2.20×10^{-3} for Cell B, respectively. It indicates that *J*_{SC} of Cell A decreased more than that of Cell B. This means that low temperature condition of -20°C , which retarded the decrease of *J*_{SC}, may be beneficial for DSSCs. On the other hand, the increase of *V*_{OC} and *FF* wasn't linear. For DSSCs, there is a trade-off between *J*_{SC} and *V*_{OC} [23]. Based on this relationship, the drop of *J*_{SC} often accompanies with the rise of *V*_{OC}.

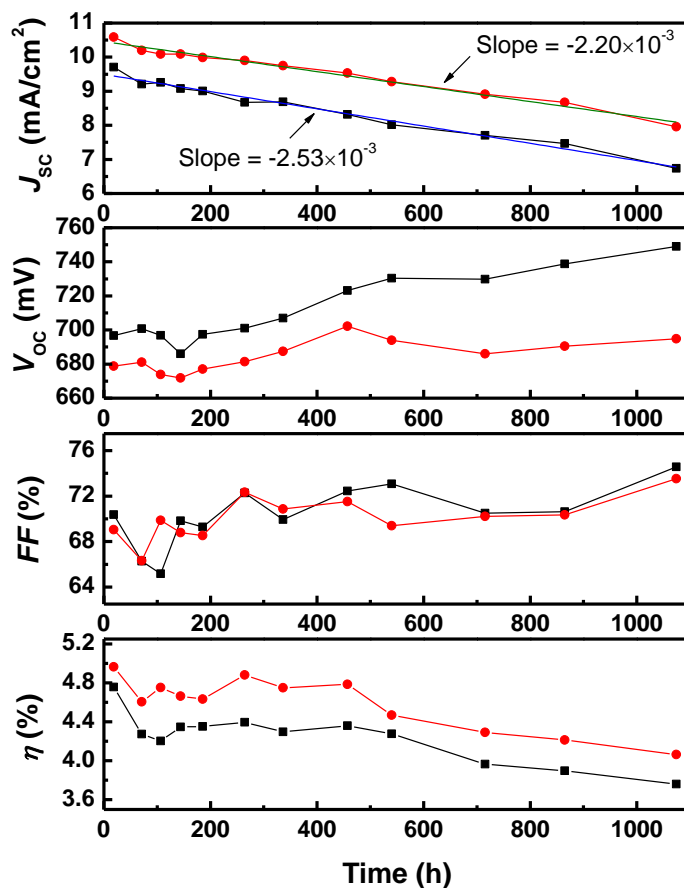


Figure 3. Evolution of *I-V* parameters for Cell A (■) and Cell B (●).

Based on the above analysis, the decrease of η was caused by the drop of J_{SC} . According to Equation 3 and the following formula,

$$IPCE(\lambda) = \eta_{LH}(\lambda)\eta_{INJ}(\lambda)\eta_{COL}(\lambda) \quad (4)$$

J_{SC} of a DCCS is determined by three factors: the light harvesting efficiency of photoelectrode (η_{LH}), the electron injection efficiency from the excited state of dye to the TiO_2 conduction band (η_{INJ}), and the electron collection efficiency of photoelectrode (η_{COL}). For a ruthenium dye adsorbed on the TiO_2 nanoparticles, the electron injection is very fast, in the femtosecond time scale [24,25], and η_{INJ} is near to 100%. Thus, the change of η_{LH} and η_{COL} is needed to be considered. On the other hand, the rise of V_{OC} and FF with time suppressed the decrease of η to some extent. In the next contexts, the reasons for the rise of V_{OC} and FF will be found.

3.2. UV-visible spectrum and resonance Raman scattering characteristics

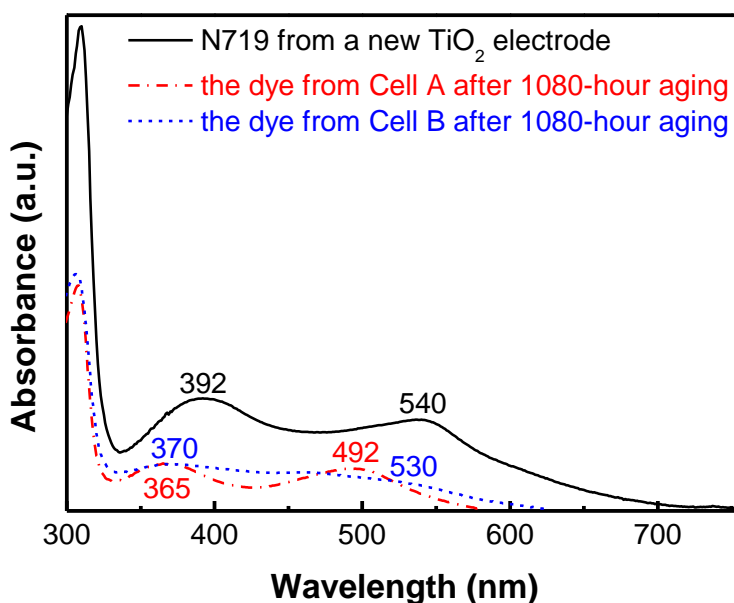


Figure 4. UV-visible absorption spectra of the dyes in a 0.05 M NaOH aqueous solution before and after 1080-hour aging.

The absorption spectra of the dyes in a 0.05 M NaOH aqueous solution were shown in Figure 4. For N719 desorbed from a new TiO_2 electrode, two broad visible bands at 540 and 392 nm are assigned to metal-to-ligand charge-transfer (MLCT) origin, and the band in the UV at 310 nm is assigned as intraligand ($\pi-\pi^*$) charge-transfer transitions [26,27]. As the aging time prolonged, the visible absorption peak of the dye desorbed from Cell A's photoelectrode blue shifted to 492 and 365 nm. Similarly, the dye desorbed from Cell B's photoelectrode showed two blue-shifted visible absorption peaks at 530 and 370 nm. Moreover, the long wavelength threshold of the absorption for N719 was at 758 nm, while the long wavelength threshold of the absorption for the dye desorbed from

Cell A and Cell B after 1080-hour aging blue shifted to 578 nm and 623 nm, respectively [28]. It indicates that the long wavelength threshold of the absorption and the visible absorption peaks of the dye desorbed from Cell A blue shifted more, in comparison to the dye desorbed from Cell B. It can be seen that the absorption peak of the dye blue shifted and the absorption spectrum of the dye narrowed with time passed by. This phenomenon suggests that N719 itself had undergone chemical reaction, which led to the widening of the dye band gap. As a result, η_{LH} decreased.

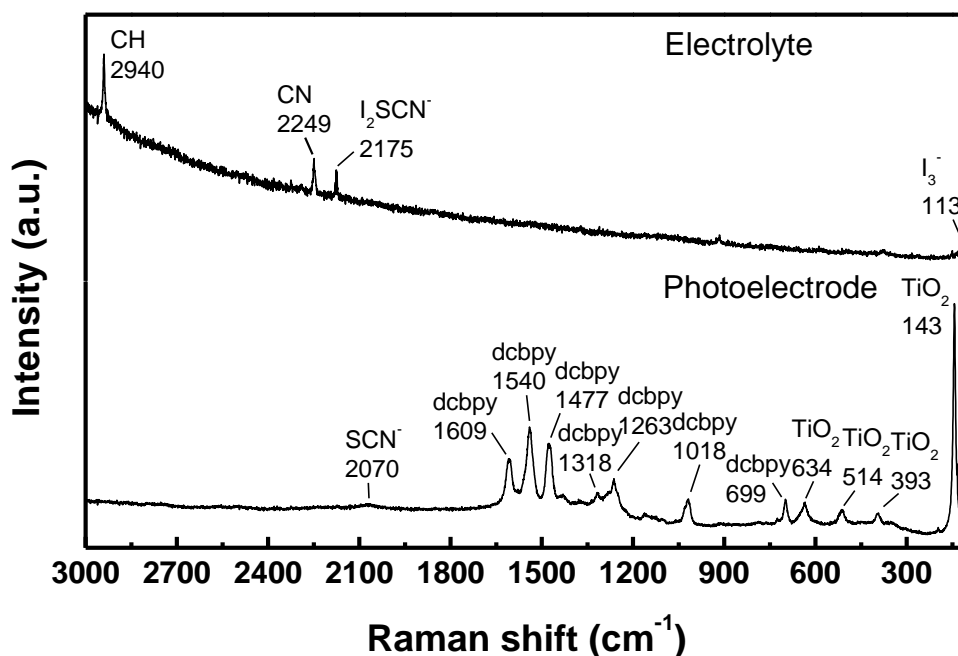


Figure 5. The Raman spectrum of Cell C at room temperature after 4 months, where dcbpy is dicarboxybipyridine group.

To further investigate the deterioration of N719, the electrolyte was extracted from Cell C at room temperature for 4 months. Subsequently, the RRS spectra of the electrolyte and the TiO_2 photoelectrode adsorbing the N719 dye were measured, as shown in Figure 5. RRS has been applied to research the causes for degradation of DSSCs at the molecular level. The Raman lines are assigned to vibrations from the different constituents in DSSCs [16,29,30]. The Raman spectra of the DSSC in Figure 5 can be divided into four frequency regions: (a) 100-670 cm^{-1} , dominated by the most intense TiO_2 modes at 143, 393, 514, and 634 cm^{-1} as well as the triiodide (I_3^-) mode at 113 cm^{-1} ; (b) 670-2000 cm^{-1} , where the main dcbpy vibrations of the dye molecules were observed at 699, 1018, 1263, 1318, 1477, 1540 and 1609 cm^{-1} ; (c) 2000-2200 cm^{-1} , displaying the thiocyanato (SCN^-) ligand vibration of the dye at 2070 cm^{-1} and the I_2SCN^- vibration in the electrolyte at 2175 cm^{-1} ; and (d) 2200-3000 cm^{-1} , where the CN vibration at 2249 cm^{-1} and the CH vibration at 2940 cm^{-1} of the acetonitrile and valeronitrile in the electrolyte existed. From the Raman spectra, it suggests that the thiocyanato ligands formed a complex with iodine, I_2SCN^- , which is considered to cause the loss of the SCN^- ligand from N719. Such a complex is regarded as an analogue of I_3^- according to



This RRS result, together with the blue shift of the visible absorption peak for the dye presented in Figure 4, suggest that the adsorbed N719 dye had become bis(tetrabutylammonium) *cis*-bis(iodo)bis(2,2'-bipyridine-4-carboxylic acid, 4'-carboxylate)ruthenium(II) (N719-I) after the SCN^- ligand loss. The ligand exchange reaction occurring in the DSSC is expressed by the following formula [16],



where $\text{Ru}(\text{dcbpy})_2(\text{SCN})_2^{2-}$ is N719, and $\text{Ru}(\text{dcbpy})_2\text{I}_2^{2-}$ is N719-I.

On the basis of the UV-visible absorption spectra in Figure 4, it suggests that for a DSSC at the higher temperature, the exchange reaction rate is faster. Since the coordination of the SCN^- to the dye is believed to be important in the reduction of the oxidized dye through getting electron from iodide (I^-) [31], the loss of SCN^- ligands will suppress the dye regeneration then reduce the short-circuit current density [32]. The exchange reaction reduced both the volume concentration of N719 adsorbed on the photoelectrode and the I_3^- concentration in the electrolyte. The decrease of the I_3^- concentration will retard the back transfer of electron from the conduction band of TiO_2 to I_3^- , and improve V_{OC} according to the formula [33,34]

$$V_{\text{oc}} = \left(\frac{kT}{q} \right) \ln \left(\frac{I_{\text{inj}}}{n_{\text{cb}} k_{\text{et}} [\text{I}_3^-]} \right) \quad (7)$$

where k and T are the Boltzmann constant and absolute temperature, respectively, q is the elementary charge, I_{inj} is the photocurrent resulting from injection, n_{cb} is the electron concentration at the conduction band of TiO_2 , k_{et} is the rate constant for the back transfer of electron, and $[\text{I}_3^-]$ is the I_3^- concentration.

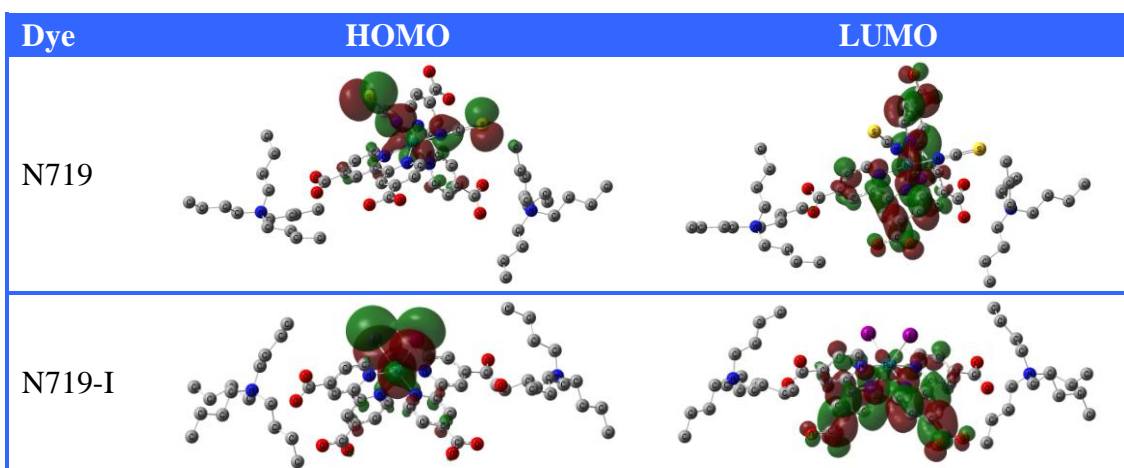
Additionally, N719 desorption from TiO_2 electrode during illumination also caused the decrease of J_{SC} for DSSCs [35]. Furthermore, the P25 TiO_2 particle is a kind of photocatalyst, which has a strong photodegradation function for N719, especially under ultraviolet light [12,36]. The illumination was provided by AM 1.5 global simulated sunlight at I - V testing and indoor diffuse light from the sun. The desorption and photodegradation of N719 also decreased η_{LH} .

3.3. DFT calculation results

Table 2 shows HOMO and LUMO distributions of N719 and N719-I. HOMO of N719 locates primarily in Ru and SCN^- ligand and marginally in dcbpy, LUMO distributes in Ru and dcbpy. The energy gap between HOMO and LUMO is 1.76 eV. After the replacement of SCN^- ligand by I^- , HOMO locates primarily in Ru and I^- and marginally in dcbpy, while LUMO resides at Ru and dcbpy.

Obviously, replacing SCN^- ligand with I^- changes the orbital composition. The energy gap between HOMO and LUMO for N719-I is 1.93 eV, which is larger than 1.76 eV of N719. This means that more energy is needed to excite the electron in HOMO to LUMO for N719-I than that for N719, which accounts well the UV-visible absorption spectrum measurement result in Figure 4. Moreover, the LUMO energy level of N719-I is higher than that of N719 by 0.15 eV. It can be anticipated the higher potential of electron injection from the excited state of N719-I to the conduction band of TiO_2 compared with N719 [37]. This condition might cause the negative shift of TiO_2 conduction band edge and induce the improvement of V_{OC} for Cell A and Cell B as the aging time prolonged.

Table 2. HOMO and LUMO distributions of N719 and N719-I.



3.4. Morphology of TiO_2 electrode films

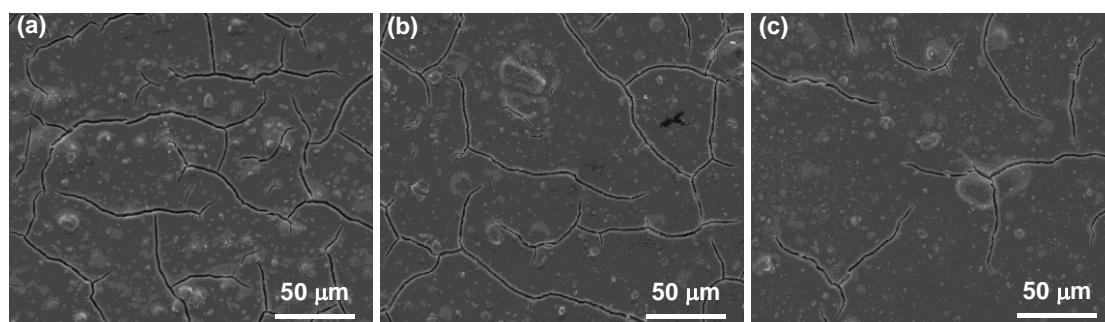


Figure 6. SEM photographs (1300 \times) for the surface morphology of TiO_2 electrode films, (a) the electrode of Cell A, (b) the electrode of Cell B, (c) a new TiO_2 electrode.

The TiO_2 electrode films of Cell A and Cell B after 1080-hour aging were observed by a scanning electron microscope, as shown in Figure 6. As a comparison, Figure 6 also shows the SEM picture of a new TiO_2 electrode film. From Figure 6, it can be found that: (1) the number of cracks in the electrode film would increase as the aging time prolonged; (2) the crack density of electrode film at high temperature was higher than that at low temperature; (3) owing to the effect of expanding with

heat and contracting with cold, the thermal stress in electrode film under the temperature cycle was larger than that at room temperature, and the cracks for Cell B were relatively broader than that for Cell A. As a statistical result of 50 counts, the average size at the most wide place of cracks was 2.11 μm for the electrode of Cell A and 2.42 μm for the electrode of Cell B, respectively. For DSSCs, the electron has a diffusion process in the porous TiO_2 photoelectrode before it arrives at the FTO substrate and enters into the external circuit. Furthermore, the electron transport among the interconnected nanocrystalline TiO_2 particles is random [38,39]. Thus, the increase of cracks in the electrode film will retard the transport of electron. Meanwhile, the increase of cracks will slightly weaken η_{LH} . Some incident light will penetrate the cracks directly and can't be utilized by the TiO_2 electrode.

3.5. EIS analysis

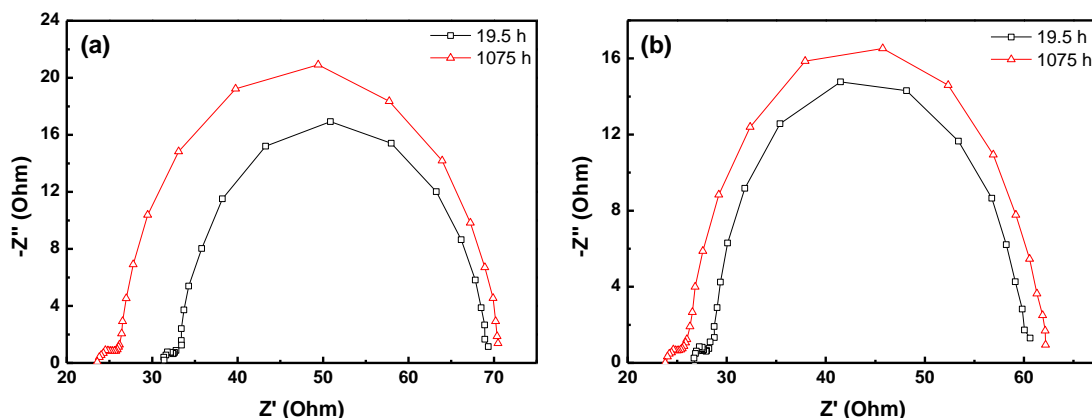


Figure 7. The EIS data of Cell A (a) and Cell B (b) at 19.5 h and 1075 h.

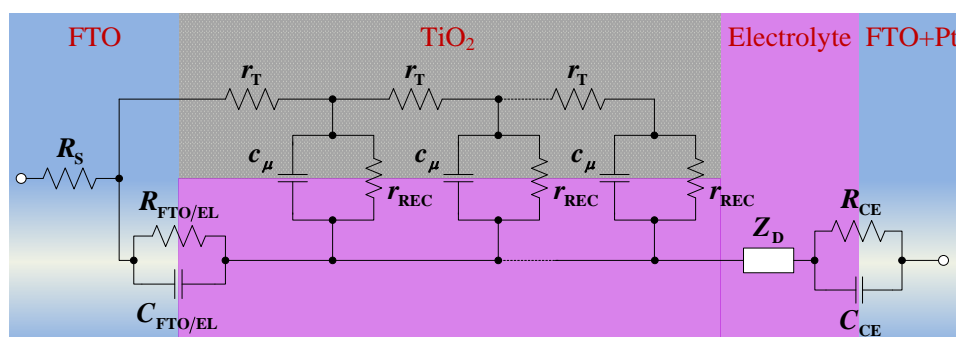


Figure 8. Transmission line model of DSSCs used to fit the experimental impedance data. r_T : transport resistance of electron in the photoelectrode film, r_{REC} and c_μ : charge transfer resistance and chemical capacitance at the $\text{TiO}_2/\text{dye}/\text{electrolyte}$ interface, $R_T = r_T d$, $R_{\text{REC}} = r_{\text{REC}}/d$, $C_\mu = c_\mu d$, where d is the TiO_2 film thickness. R_{CE} , $R_{\text{FTO/EL}}$: charge transfer resistance at the Pt counter electrode/electrolyte interface, and the FTO substrate/electrolyte interface, respectively. C_{CE} , $C_{\text{FTO/EL}}$: double layer capacitance at the Pt counter electrode/electrolyte interface, and the FTO substrate/electrolyte interface, respectively. R_S and Z_D : ohmic series resistance of the cell and mass transport impedance in the electrolyte.

EIS, which has been an effective characterization method for DSSCs research, can be used to analyze the electron transport/transfer process between the interfaces in DSSCs [40-42]. Figure 7 shows the EIS experimental data in Nyquist plots of Cell A and Cell B at 19.5 h and 1075 h. The EIS experimental data were fitted according to the transmission line model of DSSCs [43-46] presented in Figure 8.

Table 3 lists the parameters determined by fitting the EIS experimental data to the transmission line model. By comparing the data at 19.5 h with the data at 1075 h in Table 3, there are four points worthy of being paid attention to. Firstly, ohmic series resistance (R_S) of the cell became low with time, which directly caused the increase of FF [23]. Secondly, charge transfer resistance (R_{CE}) at the counter electrode/electrolyte interface increased as the aging time prolonged. This means that the Pt particle catalysts on the counter electrode suffered some degree of deactivation. Thirdly, total resistance of electron transport (R_T) in the photoelectrode film increased, which was caused by the increase of cracks in TiO_2 film with time. As shown in Figure 6, the crack density for Cell B was lower than that for Cell A, but the cracks for Cell B were relatively broader. Therefore, the increase of R_T for Cell B was higher than that for Cell A after 1080-hour aging. On the other hand, total recombination resistance (R_{REC}) at the TiO_2 /dye/electrolyte interface increased. This indicates that the back electron transfer from the TiO_2 conduction band to I_3^- was suppressed by the decrease of the I_3^- concentration resulting from the exchange reaction between I_3^- and N719. In addition, the temperature influenced the rate of the exchange reaction, thus the increase of R_{REC} for Cell A was higher than that for Cell B. Fourthly, the diffusion length of electron (L_n) representing η_{COL} [47] can be calculated by the formula $L_n = d(R_{REC}/R_T)^{1/2}$ [46]. L_n remained almost unchanged for Cell A. While for Cell B, η_{COL} decreased slightly due to the minute decrease of L_n . Thus, the decrease of J_{SC} for the two cells was mainly attributed to the decrease of η_{LH} according to Equation 4.

Table 3. Parameters determined by fitting the EIS experimental data to the transmission line model.

Device	d (μm)	Duration of time (h)	R_S (Ω)	R_{CE} (Ω)	R_T (Ω)	R_{REC} (Ω)	L_n (μm)
Cell A	7.6	19.5	31.3	1.63	3.68	33.7	23.0
		1075	23.6	2.98	4.45	41.5	23.2
Cell B	10	19.5	26.6	1.45	3.34	29.7	29.8
		1075	23.9	1.91	4.56	33.1	27.0

4. CONCLUSIONS

In this work, a long-term stability testing of DSSCs under two different temperature conditions was performed. From stability of N719, aging of the TiO_2 photoelectrode film, change of the electrolyte components, and degradation of the counter electrode, the decrease of conversion efficiency for DSSCs was investigated. The following conclusions can be drawn reasonably: (1) The decrease of η for DSSCs was attributed to the decrease of J_{SC} which was mainly caused by the decrease of η_{LH} . J_{SC}

and η of the cell at 25°C decreased more compared with the cell under the temperature cycle from -20°C to 25°C. N719 adsorbed on the TiO₂ electrode is not stable, it can react with I₃⁻ in the electrolyte and be desorbed or photodegraded under illumination, which leads to the decrease of η_{LH} . Moreover, high temperature will accelerate the exchange reaction rate. The stability of N719 in dye-sensitized solar cell system is a crucial factor for the long-term performance of DSSCs. (2) The increase of V_{OC} and FF suppressed the decrease of η to some extent. V_{OC} of the cell at 25°C increased more compared with the cell under the temperature cycle from -20°C to 25°C, and the increase of FF was almost the same for the two temperature conditions. The increase of the V_{OC} was attributed to the decrease of the I₃⁻ concentration and a negative shift of the conduction band edge of TiO₂ after N719 deteriorated. (3) After 1080-hour aging, the cracks in the TiO₂ electrode film increased in number, which would slightly weaken η_{LH} and retard the electron diffusion to the FTO substrate. On the other hand, the decrease of the I₃⁻ concentration suppressed the back electron transfer from the TiO₂ conduction band to I₃⁻. Combining these two factors, the change of η_{COL} with time was not large. (4) The effect of expanding with heat and contracting with cold decreased η_{COL} to some extent, but the low temperature postponed the deterioration of N719. For DSSCs under the temperature cycle from -20°C to 25°C, the low temperature will suppress the decrease of photovoltaic performance. These conclusions should be helpful to some extent for the improvement and application of DSSCs.

ACKNOWLEDGMENTS

This work is financially supported by the National Natural Science Foundation of China (Grant Nos. 11174129, 51102132 and 21073090), the National Basic Research Program of China (Grant No. 2011CB933303), the Jiangsu Provincial Science and Technology Research Program (Grant No. BK2011056). PhD Yongjun Yuan, Jing Chen, and Jian Gao at Nanjing University are thanked for discussions.

References

1. B. Oregan and M. Grätzel, *Nature*, 353 (1991) 737.
2. D. Wei and G. Amaratunga, *Int. J. Electrochem. Sci.*, 2 (2007) 897.
3. M. H. Lai, M. W. Lee, G. J. Wang and M. F. Tai, *Int. J. Electrochem. Sci.*, 6 (2011) 2122.
4. A. Yella, H. W. Lee, H. N. Tsao, C. Y. Yi, A. K. Chandiran, M. K. Nazeeruddin, E. W. G. Diau, C. Y. Yeh, S. M. Zakeeruddin and M. Grätzel, *Science*, 334 (2011) 629.
5. E. Figgemeier and A. Hagfeldt, *Int. J. Photoenergy*, 6 (2004) 127.
6. M. I. Asghar, K. Miettunen, J. Halme, P. Vahermaa, M. Toivola, K. Aitola and P. Lund, *Energ. Environ. Sci.*, 3 (2010) 418.
7. M. Grätzel, *Cr. Chim.*, 9 (2006) 578.
8. M. Toivola, J. Halme, L. Peltokorpi and P. Lund, *Int. J. Photoenergy*, (2009), DOI: 10.1155/2009/786429.
9. A. Hinsch, J. M. Kroon, R. Kern, I. Uhlendorf, J. Holzbock, A. Meyer and J. Ferber, *Prog. Photovoltaics*, 9 (2001) 425.
10. S. Y. Dai, J. Weng, Y. F. Sui, S. H. Chen, S. F. Xiao, Y. Huang, F. T. Kong, X. Pan, L. H. Hu, C. N. Zhang and K. J. Wang, *Inorg. Chim. Acta*, 361 (2008) 786.
11. Y. Takeda, N. Kato, K. Higuchi, A. Takeichi, T. Motohiro, S. Fukumoto, T. Sano and T. Toyoda, *Sol. Energ. Mat. Sol. C.*, 93 (2009) 808.

12. H. Pettersson and T. Gruszecki, *Sol. Energ. Mat. Sol. C.*, 70 (2001) 203.
13. H. Matsui, K. Okada, T. Kitamura and N. Tanabe, *Sol. Energ. Mat. Sol. C.*, 93 (2009) 1110.
14. P. M. Sommeling, M. Spath, H. J. P. Smit, N. J. Bakker and J. M. Kroon, *J. Photoch. Photobio. A*, 164 (2004) 137.
15. N. Kato, Y. Takeda, K. Higuchi, A. Takeichi, E. Sudo, H. Tanaka, T. Motohiro, T. Sano and T. Toyoda, *Sol. Energ. Mat. Sol. C.*, 93 (2009) 893.
16. H. Greijer, J. Lindgren and A. Hagfeldt, *J. Phys. Chem. B*, 105 (2001) 6314.
17. S. Ito, P. Chen, P. Comte, M. K. Nazeeruddin, P. Liska, P. Pechy and M. Grätzel, *Prog. Photovoltaics*, 15 (2007) 603.
18. A. D. Becke, *J Chem Phys*, 98 (1993) 5648.
19. C. T. Lee, W. T. Yang and R. G. Parr, *Phys. Rev. B*, 37 (1988) 785.
20. M. J. Frisch, G. W. Trucks, H. B. Schlegel, G. E. Scuseria, M. A. Robb, J. R. Cheeseman, et al. Gaussian 03, Revision E.01, Gaussian Inc.: Wallingford, CT, 2004.
21. L. Q. Xiong, Q. Zhao, H. L. Chen, Y. B. Wu, Z. S. Dong, Z. G. Zhou and F. Y. Li, *Inorg. Chem.*, 49 (2010) 6402.
22. M. Ni, M. K. H. Leung and D. Y. C. Leung, *Can. J. Chem. Eng.*, 86 (2008) 35.
23. N. Koide, A. Islam, Y. Chiba and L. Y. Han, *J. Photoch. Photobio. A*, 182 (2006) 296.
24. G. Benko, J. Kallioinen, J. E. I. Korppi-Tommola, A. P. Yartsev and V. Sundstrom, *J. Am. Chem. Soc.*, 124 (2002) 489.
25. S. A. Haque, E. Palomares, B. M. Cho, A. N. M. Green, N. Hirata, D. R. Klug and J. R. Durrant, *J. Am. Chem. Soc.*, 127 (2005) 3456.
26. M. J. Root, B. P. Sullivan, T. J. Meyer and E. Deutsch, *Inorg. Chem.*, 24 (1985) 2731.
27. M. K. Nazeeruddin, S. M. Zakeeruddin, R. Humphry-Baker, M. Jirousek, P. Liska, N. Vlachopoulos, V. Shklover, C. H. Fischer and M. Grätzel, *Inorg. Chem.*, 38 (1999) 6298.
28. H. G. Agrell, J. Lindgren and A. Hagfeldt, *Sol. Energy*, 75 (2003) 169.
29. H. G. Agrell, J. Lindgren and A. Hagfeldt, *J. Photoch. Photobio. A*, 164 (2004) 23.
30. T. Stergiopoulos, A. G. Kontos, V. Likodimos, D. Perganti and P. Falaras, *J. Phys. Chem. C*, 115 (2011) 10236.
31. H. Rensmo, S. Sodergren, L. Patthey, K. Westermark, L. Vayssieres, O. Kohle, P. A. Bruhwiler, A. Hagfeldt and H. Siegbahn, *Chem. Phys. Lett.*, 274 (1997) 51.
32. J. R. Jennings, Y. R. Liu and Q. Wang, *J. Phys. Chem. C*, 115 (2011) 15109.
33. M. K. Nazeeruddin, A. Kay, I. Rodicio, R. Humphrybaker, E. Muller, P. Liska, N. Vlachopoulos and M. Grätzel, *J. Am. Chem. Soc.*, 115 (1993) 6382.
34. C. N. Zhang, S. H. Chen, H. J. Tian, Y. Huang, Z. P. Huo, S. Y. Dai, F. T. Kong and Y. F. Sui, *J. Phys. Chem. C*, 115 (2011) 8653.
35. H. S. Uam, Y. S. Jung, Y. Jun and K. J. Kim, *J. Photoch. Photobio. A*, 212 (2010) 122.
36. Y. X. Chen, K. Wang and L. P. Lou, *J. Photoch. Photobio. A*, 163 (2004) 281.
37. C. F. Lo, S. J. Hsu, C. L. Wang, Y. H. Cheng, H. P. Lu, E. W. G. Diau and C. Y. Lin, *J. Phys. Chem. C*, 114 (2010) 12018.
38. J. Nelson, *Phys. Rev. B*, 59 (1999) 15374.
39. J. van de Lagemaat and A. J. Frank, *J. Phys. Chem. B*, 105 (2001) 11194.
40. T. Hoshikawa, M. Yamada, R. Kikuchi and K. Eguchi, *J. Electrochem. Soc.*, 152 (2005) E68.
41. F. Fabregat-Santiago, E. M. Barea, J. Bisquert, G. K. Mor, K. Shankar and C. A. Grimes, *J. Am. Chem. Soc.*, 130 (2008) 11312.
42. L. Andrade, S. M. Zakeeruddin, M. K. Nazeeruddin, H. A. Ribeiro, A. Mendes and M. Graetzel, *Chemphyschem*, 10 (2009) 1117.
43. J. Bisquert, *J. Phys. Chem. B*, 106 (2002) 325.
44. Q. Wang, S. Ito, M. Grätzel, F. Fabregat-Santiago, I. Mora-Sero, J. Bisquert, T. Bessho and H. Imai, *J. Phys. Chem. B*, 110 (2006) 25210.
45. M. Adachi, M. Sakamoto, J. T. Jiu, Y. Ogata and S. Isoda, *J. Phys. Chem. B*, 110 (2006) 13872.

46. J. Halme, P. Vahermaa, K. Miettunen and P. Lund, *Adv. Mater.*, 22 (2010) E210.

47. J. Halme, G. Boschloo, A. Hagfeldt and P. Lund, *J. Phys. Chem. C*, 112 (2008) 5623.

© 2012 by ESG (www.electrochemsci.org)